Article

**Journal of
Nanoscience and Nanotechnology**
Vol. 14, 7325–7332, 2014
www.aspbs.com/jnn

Photo-Catalyzed *p*-Nitrophenol Degradation in Aqueous Dispersions of Ferrihydrite and H_2O_2

Yongjuan Wu[1,2,3,4], Rufen Chen[3], Hui Liu[3], Yu Wei[3,*], and Dong Wu[1]

[1] *Institute of Coal Chemistry, Chinese Academy of Sciences, Taiyuan 030001, China*
[2] *University of Chinese Academy of Sciences, Beijing 100049, China*
[3] *Key Laboratory of Inorganic Nanommaterials of Hebei Province, Hebei Normal University, Shijiazhuang 050086, China*
[4] *Huihua College of Hebei Normal University, Shijiazhuang 050091, China*

Nitrophenols are hazardous and toxic to living organisms. For this study, ferrihydrite was prepared to test its capabilities for *p*-nitrophenol degradation. A ferrihydrite particle prepared in neutral environmental conditions is sphere-like with a diameter of 2–4 nm and its total surface area is approximately 229 $m^2 \cdot g^{-1}$. The combination of ferrihydrite and trace H_2O_2 is effective for the degradation of *p*-nitrophenol under simulated sunlight irradiation. Hydroquinone, the initial intermediate of *p*–nitrophenol decomposition, autocatalyses the subsequent degradation of *p*-nitrophenol because it accelerates the photo-reductive dissolution of ferrihydrite. The effect of key operating parameters such as ferrihydrite dosage, initial solution pH and H_2O_2 dosage were also studied on the photocatalytic degradation of *p*-nitrophenol. The results indicate that the combination of 0.2 $g \cdot L^{-1}$ ferrihydrite, 0.45 $mmol \cdot L^{-1}$ H_2O_2 is highly efficient for the degradation of *p*-nitrophenol (0.15 $mmol \cdot L^{-1}$) at pH 2.5∼3.0. A ferrihydrite was reused several times, still keeping its original photocatalysis.

Keywords: Photocatalysis, *p*-Nitrophenol, Ferrihydrite, H_2O_2.

1. INTRODUCTION

p-Nitrophenol (*p*-NP) is a highly toxic, stable, and biorefractory chemical in the environment due to the presence of a nitro-group in the aromatic ring. It widely exists in industrial wastes derived from farm chemicals, pharmaceuticals, and synthetic dyes. Current technologies for the removal of *p*-NP include physical (e.g., screening, mixing, flocculation, sedimentation, floatation, filtration, microwave, radiation, extraction, adsorption, etc.), biological (e.g., biodegradation), and chemical (e.g., electrochemistry, precipitation, photocatalysis, disinfection, chemical oxidation, etc.) methods. Combination of these different methods has been used to achieve more efficient degradation of organic compounds.[1–3] Advanced oxidation processes (AOPs) such as O_3/H_2O_2,[4] O_3/UV,[5] UV/H_2O_2,[6] Fe^{2+}/H_2O_2,[7] and photocatalytic oxidation[8–13] are known to be effective for the decomposition of organic compounds. These processes are based on the generation of reactive oxygen species such as hydroxyl radicals ($^{\bullet}OH$) that react with many organic compounds. Among the AOPs, Fenton (Fe^{2+}/H_2O_2) and Fenton-like processes are some of the most attractive methods because their reagents are environmentally benign and abundant in the earth's crust.[14] Previous studies[15–17] have described the degradation of organic pollutants in Fenton or Fenton-like processes. Few reports have been found for the degradation of *p*-NP in a Fenton-like processes under solar light irradiation.

Ferrihydrite (FH), a poorly crystalline Fe(III) oxyhydroxid, is a common Fe(III) (hydr)oxide in soils and sediments undergoing fluctuating redox conditions.[18] Due to its high surface area and intrinsic reactivity, ferrihydrite serves as a dominant sink for numerous metals (e.g., As) and nutrients (e.g., P). Ferrihydrite is also considered the most (bio) available Fe(III) (hydr)oxide for dissimilatory iron-reducing bacteria (DIRB) and thus greatly influences the global cycling of carbon.[19]

As we know, the method reported by Cornell and Schwertmann (2003)[20] has been the method mainly used for the preparation of FH in references. Briefly, alkaline solution was added into Fe^{3+} solution to adjust the pH value to 7–8. In this process, the formation of FH went

---

[*] Author to whom correspondence should be addressed.

1533-4880/2014/14/7325/008 doi:10.1166/jnn.2014.8979

through a pH change from acidic to neutral. However, FH occurs in many environments from environmental to alkaline conditions.[21, 22]

Here FH was prepared by simulating environmental conditions. The process of *p*-NP oxidative decomposition in the presence of ferrihydrite and trace H_2O_2 under solar light irradiation, factors such as FH dosage, initial solution pH and H_2O_2 dosage on the photocatalytic degradation of *p*-NP and the reusability of FH were investigated in detail. These results may provide useful information on the migration of nitrophenols through an abiotic or biotic process.

2. MATERIALS AND METHODS

2.1. Materials

Ferric nitrate ninehydrate [$Fe(NO_3)_3 \cdot 9H_2O$], sodium hydroxide (NaOH), *p*-nitrophenol and H_2O_2 were of analytical purity. Distilled water was used. The ferric salt solution was filtered through a 0.22 μm millipore filter to eliminate any particulate contaminants.

2.2. Preparation of Ferrihydrite

NaOH solution ($6.0\ \text{mol} \cdot \text{L}^{-1}$) and $Fe(NO_3)_3$ solution (25 mL, $2.0\ \text{mol} \cdot \text{L}^{-1}$) were added simultaneously into certain water at RT under stirring. The rate of adding two solutions was controlled by maintaining pH 7 with accuracy of better than 0.5 pH units. The agitation was continued for an additional 30 min until the pH was adjusted to a stable one by adding NaOH (1.0 M). At the same time the total volume of the system was adjusted to 100 mL. In this system, a gel-like deposit was formed. The product was filtered and washed thoroughly with distilled water and then dried at about 40 °C for 12 h.

2.3. Photocatalytic Oxidation Process

All experiments were carried out in a pyrex glass vessel with a water jacket at (298 ± 0.5) K. Aqueous suspensions were prepared by adding FH powder to *p*-NP [$0.15\ \text{mmol} \cdot \text{L}^{-1}$ (mM), 100 mL] solution. The suspension pH was adjusted with NaOH or HCl to keep deviation within 0.02 pH units. Prior to irradiation, the suspensions were magnetically stirred in the dark for 1 h to establish the adsorption/desorption equilibrium between *p*-NP and FH particles. It is noteworthy that the amount of *p*-NP physically adsorbed on FH was lower than 2% of the initial one. So the adsorbed *p*-NP was neglected. Subsequently, the Fenton-like reaction was started with the introduction of hydrogen peroxide (H_2O_2) and irradiation simultaneously. A General electric ELH projection lamp, 200 W/120 V, was used as the light source at an intensity of $700\ \text{W} \cdot \text{m}^{-2}$. These lamps provide an illumination spectrum similar to sunlight (380–780 nm). Samples were periodically taken and filtered through a 0.22 μm millipore filter. The concentration of *p*-NP was measured by HPLC at 317 nm.

In some case, superadded reaction (SR) was immediately followed by photocatalysis above. Briefly, after photocatalysis was completed, a *p*-NP solution with certain volume and concentration was superadded into the operating batch reactors to sustain *p*-NP solution as 0.15 mM, 100 mL. Other steps were the same as first circle of photocatalysis.

To test the regeneration and reusability of FH, another photocatalytic oxidation of *p*-NP was followed after the first circle of photocatalysis. Namely, after the first five hours of photocatalytic oxidation of *p*-NP in FH/H_2O_2 dispersion, the final reaction mixture was separated using centrifuge. The supernate was decanted after a final analysis of *p*-NP concentration. The sludge was then mixed with 30 mL of $0.01\ \text{mol} \cdot \text{L}^{-1}$ NaOH and shaken at 150 rpm in a constant temperature shaker at 298 K for 1 h to make FH regeneration.[23, 24] The regenerated FH was washed with distilled water several times for the next circle of photocatalysis. Here explained that only a final analysis for *p*-NP concentration was carried out to avoid the loss of FH during each circle of photocatalytic oxidation.

2.4. Characterization and Analysis

Transmission electron microscopy (TEM) observation of samples was carried out on a JEM 2010 electron microscope (Tokyo, Japan). X-ray diffraction (XRD) measurement was performed on a D8-Advance XRD diffractometer (Bruker, German) at a scan rate of $4°\ 2\theta\ \text{min}^{-1}$ from 10° to 80° with Cu Kα target. Surface area measurements were taken with a Brunauer, Emmett, Teller (BET) (Coulter SA-3100, USA) analyzer at liquid nitrogen temperature using conventional gas adsorption apparatus. Total organic carbon (TOC) analysis was carried out by means of a Shimadzu TOC-V CPH total organic carbon analyzer. Following the method described in Ref. [25] the infrared (IR) spectroscopy (FTIR–8900) was used to monitor the course of the photo-induced conversion of *p*-NP in ferrihydrite/H_2O_2 dispersion. Namely, dispersions of pre- and post-reaction were extracted, filtered and added into vessels with KBr powder to form homogeneous solutions. Then they were dried at 40 °C under vacuum for final analysis of IR spectroscopy. The concentration of H_2O_2 was determined using a photo metric method, in which *N*,*N*-diethyl-*p*-phenylenediamine (DPD) is oxidized through a peroxidase catalyzed reaction.[26] Ferrous iron was determined spectrophotometrically using a modified phenanthroline method; the detection limit was 8 mM.[27]

3. RESULTS AND DISCUSSION

3.1. Characterization of Ferrihydrite

The position and intensity of the XRD peaks of FH confirms that the analysis sample is 2-line ferrihydrite (Fig. 1(a)), and is consistent with the results calculated by Drits et al.[28] The mesoporous structure of FH has been confirmed by N_2 adsorption/desorption isotherms

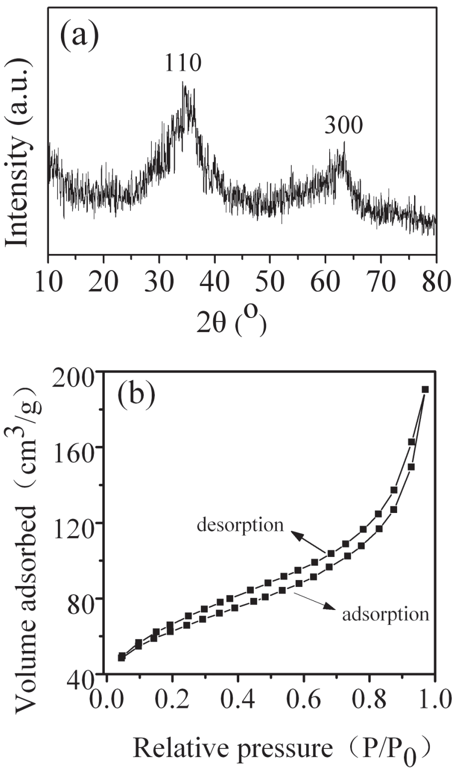

Figure 1. XRD pattern (a) and nitrogen adsorption/desorption isotherms (b) of FH.

(Fig. 1(b)). The sample presents type III isotherm (definition by IUPAC),[29] and this is a characteristic of mesoporous material. The appearance of type H-4 hysteresis loop in the isotherm indicates the presence of slot pores in the mesoporous FH.[30] N_2 sorption analysis shows that the total and external surface surface areas of FH are 228.83 $m^2 \cdot g^{-1}$ and 158.97 $m^2 \cdot g^{-1}$, respectively. The mean pore size and total pore volume are 16.38 nm and 69.85 $cm^3 \cdot g^{-1}$, respectively (Table I).

FH particle is small and easy to aggregation together. However, the single FH particle and the stripe of its crystal lattice can be made out from the edge of the aggregation unit in the high resolution transmission electron microscopy (HRTEM) image (Fig. 2(a)). FH particles are sphere-like nanosheets with a diameter of 2–4 nm. The electron diffraction pattern of FH (ED_{FH}) is diffraction ring instead of diffraction spot (Fig. 2(b)), indicating that FH sample has polycrystalline structure. Calibration results of ED_{FH}, the miller indices of the brighter and darker diffraction rings are 110 and 300, respectively. These results are consistent with the crystalline planes of XRD peaks.

Table I. Main characteristics of FH.

Parameters	Value
BET surface area ($m^2 \cdot g^{-1}$)	228.83
Total pore volume ($cm^3 \cdot g^{-1}$)	69.85
Microporel volume ($cm^3 \cdot g^{-1}$)	0.036
Exterior surface area ($m^2 \cdot g^{-1}$)	158.97
Average pore width (nm)	16.38

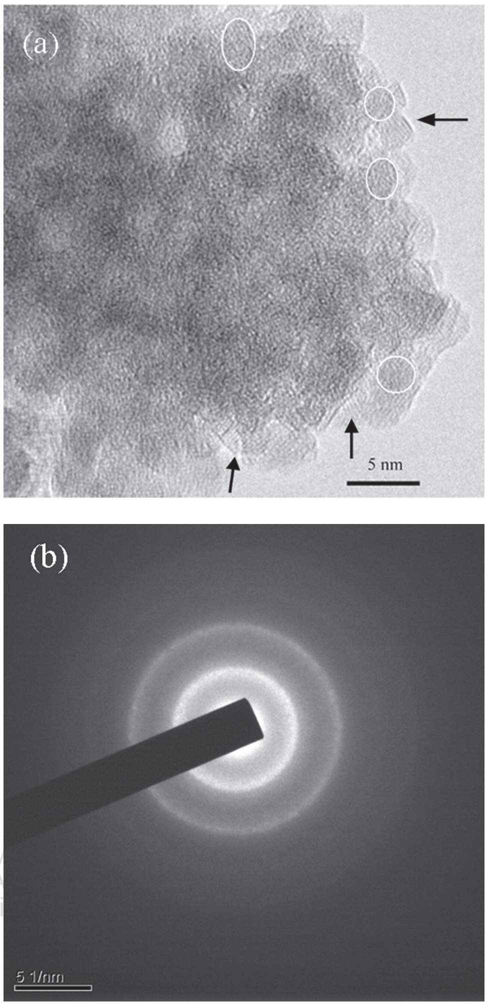

Figure 2. HRTEM image (a) and electron diffraction pattern of FH.

3.2. Photocatalytic Oxidation Study

3.2.1. Photocatalytic *p*-NP Degradation in FH/H_2O_2 Dispersion

Control experiments are carried out using only H_2O_2 or FH under irradiation (Figs. 3(a) and (b), respectively) or the combination of FH and H_2O_2 in the dark (Fig. 3(c)). The results of Figures 3(a)–(c) show negligible degradation of the substrate within the given timescale. The decomposition rate of *p*-NP notably increases under the same conditions as Figure 3(c) except for under irradiation (Fig. 3(d)). After 5 h of irradiation, 95.5% of *p*-NP are decomposed when the molar ratio of H_2O_2 to the substrate ($M_{H/S}$) is 3:1, far below the H_2O_2 dosage reported in Ref. [31] ($M_{H/S} = 1300{:}1$ in the dark) and Ref. [32] ($M_{H/S} = 15{:}1$ under ultraviolet irradiation). Therefore, the photocatalytic decomposition of *p*-NP was investigated in detail in FH/H_2O_2 dispersion.

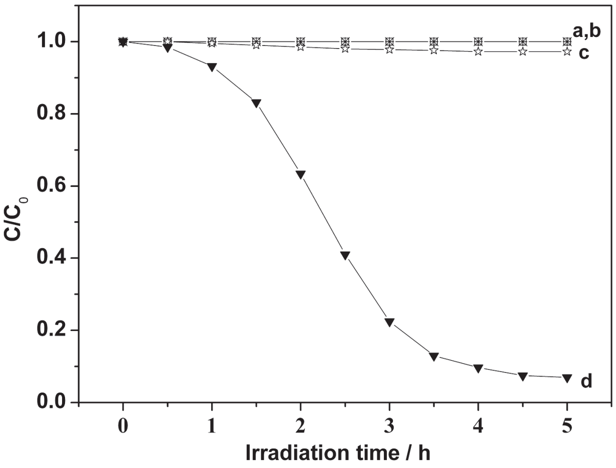

Figure 3. Changes of *p*-NP concentration versus reaction time at pH 3. Adding 0.45 mM H_2O_2 under irradiation (a); adding 0.2 $g \cdot L^{-1}$ FH under irradiation (b); coexistence of 0.2 $g \cdot L^{-1}$ FH and 0.45 mM H_2O_2 in the dark (c); coexistence of 0.2 $g \cdot L^{-1}$ FH and 0.45 mM H_2O_2 under irradiation (d).

The normalised concentration profiles displays a lag phase followed by a fast phase where the decomposition rate of *p*-NP substantially increased from 8% at 1 h to 90% at 3.5 h (Fig. 4(a)). The decomposition rate (95.5%) of *p*-NP was significantly higher than the removal rate of TOC (17.5%) after 5 h of irradiation, indicating that most *p*-NP is decomposed into organic intermediates rather than completely oxidized into CO_2 and H_2O. The TOC removal rate increases from 17.5% to 24% with increased irradiation from 5 h to 8 h, indicating the further mineralization of organic intermediates.

Infrared spectroscopy was also used to monitor the evolution of the photo-induced conversion of *p*-NP. As shown in Figure 4(b), the principal bands at 1500–1670 cm^{-1} correspond to the aromatic ring vibration of *p*-NP. They are not obviously changed before and after irradiation, indicating that there exist a large number of aromatic rings. During the photo-oxidation, the characteristic band of the nitro group (1335 cm^{-1}) disappears coupled with a notable increase of nitrate absorption peak (1380 cm^{-1}) after 5 h of irradiation. The C–O vibration of phenol at 1250–1000 cm^{-1} weakens, indicating that the phenol structure is partly destroyed. The IR results clearly illustrated that the nitro group and part of the phenol structure were destroyed with the formation of nitrate.

The changes of Uv-Vis absorption spectra are shown in Figure 2(c). The characteristic absorption band of *p*-NP is at 317 nm. The absorption band at 225–265 nm is assigned to nitro group. The peak at 204 nm is ascribed to characteristic absorption of phenyl ring. The absorption peaks at 317 nm and 227–238 nm obviously weaken as irradiation go on, indicating the decomposition of *p*-NP and the removal of nitro group. The absorptions at 200–220 nm and 238–260 nm exhibit an increment followed by a decrement along with the reaction time. The increment may be due to the ring opening to generate low-molecular-weight acids, e.g., maleic acid. These species have characteristic absorption in these regions.[33,34]

The pH obviously decreased from 3.00 to 2.10 during the first 6 h of irradiation, and then slowly increased from 2.10 to 2.14 during the subsequent irradiation (Fig. 4(d)). The decrement of pH is ascribed to the hydrolysis of newly generated Fe(III) species from reaction (1) and the generation of low-molecular-weight organic acids from *p*-NP degradation. The slight increment of pH is due to the mineralization of organic acids.

$$\mathrm{Fe(II)} + H_2O_2 \rightarrow \mathrm{Fe(III)} + {}^{\bullet}OH + OH^- \qquad (1)$$

Changes in the Fe(II) and H_2O_2 concentrations were also observed during the photoreaction (Fig. 4(e)). The concentration of Fe(II) slowly increases within 1 h while it sharply increases to 76.6 and 170 μM at 4 and 5 h, about two times of that at 2 and 4 h respectively. Accordingly, the concentration of H_2O_2 straightly decreases from 450 μM to 20 μM coupled with *p*-NP degradation.

The initial intermediate of *p*-NP decomposition is hydroquinone (HQ) and its corresponding retention time (T_R) is about 2.510 min (Figs. 5(a)–(b)). No catechol appears ($T_R = 3.991$ min, Fig. 5(c)) during *p*-NP decomposition. The peaks at $T_R = 1.574$–2.008 min ascribed to lower molecular organic acids (Fig. 5(a)).[1] The peak at $T_R = 2.320$ min ascribes to an impurity (Figs. 5(a)~(c)).

Previous studies have provided strong evidence that some phenolic intermediates can reduce aqueous Fe^{3+} to Fe^{2+} without special irradiation to accelerate the degradation of nitroaromatic compound.[17,35] Here HQ was the initial intermediate of *p*-NP decay and the concentration of Fe(II) increased as the reaction went on (shown in Fig. 2(e)). To understand the role of HQ and FH, several groups of control experiments were designed.

As shown in Figure 6, HQ is ineffective for the degradation of *p*-NP without H_2O_2 (SR-a, Fig. 6). About 10% *p*-NP was decomposed from FH/H_2O_2 dispersion in the dark after 5 h (SR-b, Fig. 6). Under the same experimental conditions as SR-b, Figure 6 except under irradiation, the lag phase disappeared within 1 h and the degradation rate of *p*-NP increased linearly from the initial irradiation to reaction termination in the superadded reaction (SR-c, Fig. 6).

To confirm the role of the initial intermediate, extra HQ (0.03 mM) was added into the present photo-catalyzed FH/H_2O_2. As shown in Figure 7, Extra addition of HQ noticeably accelerates the degradation of *p*-NP. *p*-NP concentration sharply decreases within 2 h in comparison with that without extra addition of HQ (Fig. 3(d)), and the Fe(II) concentration also linearly increases up.

The results of Figures 6–7 provided strong evidence that the HQ generated in the initial phase accelerated the subsequent degradation of *p*-NP due to its accelerating the photoreductive dissolution of Fe(III).

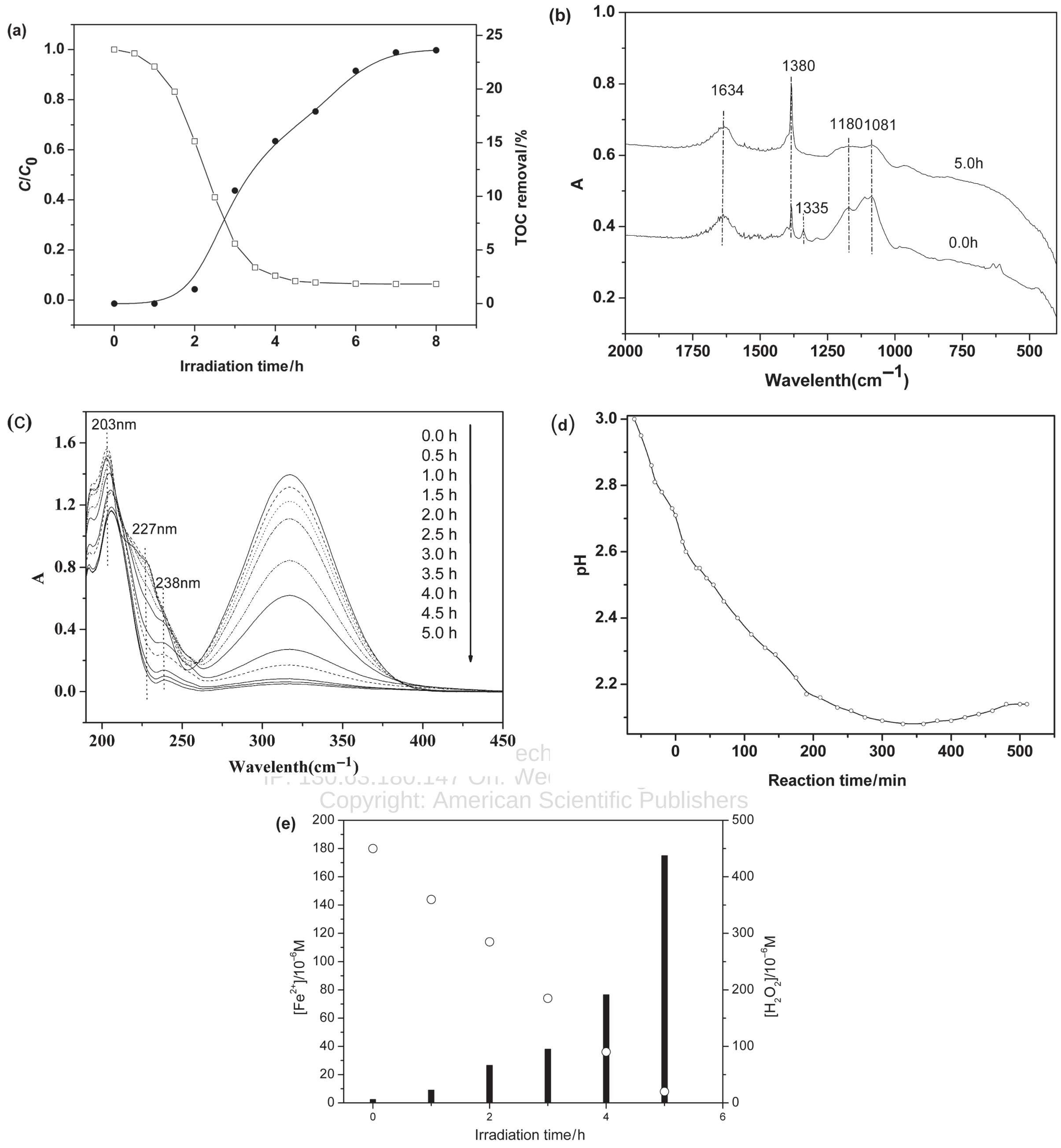

Figure 4. Changes of TOC and *p*-NP concentration (a); IR spectra of the samples at different irradiation time (b); Uv-vis absorption spectra for *p*-NP (c); pH variation (d); changes of Fe(II) concentration (filled columns) and H_2O_2 (open circles) (e).

3.2.2. Effect of Catalyst FH

The photocatalytic degradation of many pollutants is a function of the catalyst dosage.[32] To investigate the effect of the FH dosage on *p*-NP removal, several experiments were performed with varied loads from 0.1 $g \cdot L^{-1}$ to 0.5 $g \cdot L^{-1}$ in the presence of H_2O_2 (0.45 mM) under irradiation at pH 3 (Fig. 8). At 4.5 h, 83%, 95%, and 83% of *p*-NP disappears when the FH dosage is 0.1–0.3 $g \cdot L^{-1}$, respectively. However, the decomposition rate (65%) of *p*-NP obviously decreases when 0.5 $g \cdot L^{-1}$ FH is loaded due to the face that too many photons were blocked to penetrate inner side of the solid particles with an increase of FH dosage.[37] Moreover, FH was also more prone to aggregation with large dosage of FH, leading to a decrease of effective catalyst. Considering the ideal *p*-NP degradation, 0.2 $g \cdot L^{-1}$ FH was chosen as the optimal dosage for further experiments.

3.2.3. Effect of pH

Under the given experimental conditions, the effect of pH on *p*-NP degradation is illustrated in Figure 9. The decomposition rate of *p*-NP at 5 h follows the precedence

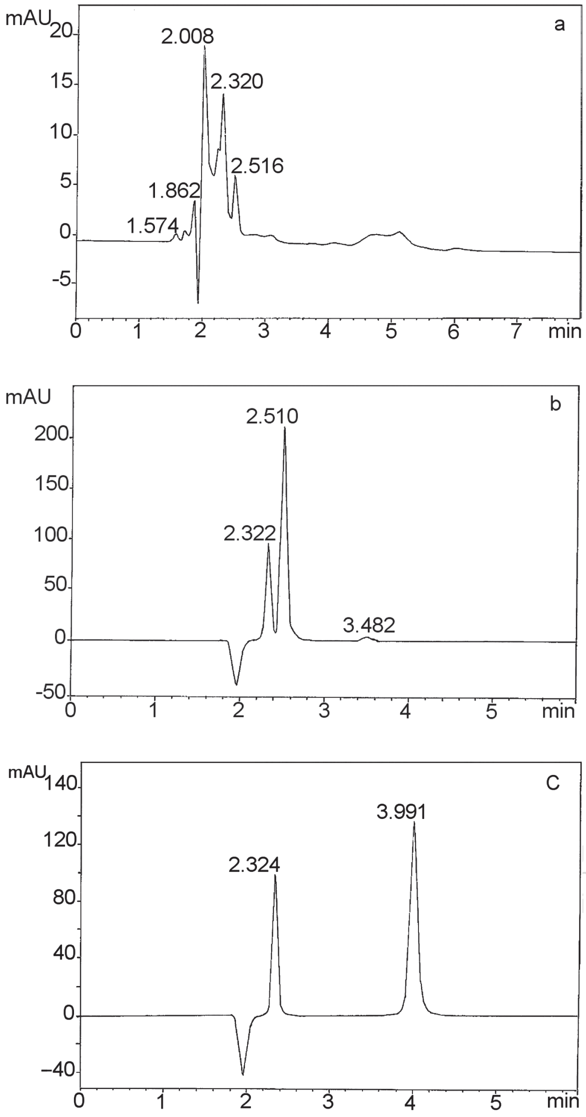

Figure 5. HPLC chromatograms of (a) post-reaction sample; (b) standard hydroquinone; (c) standard catechol.

relationship: pH 2.5 ≈ pH 3.0 (95.5%) pH > 2.0 (55%) >> pH 3.5 (30%) > pH 4.0 (15%) > pH 5.0 (0%). The highest value of *p*-NP degradation occurs at pH 2.5–3.0, and is consistent with that reported in Refs. [32, 33].

3.2.4. Effect of H_2O_2 Dosage

The H_2O_2 dosage is a key factor in the photo-degradation of *p*-NP in the FH/H_2O_2 system (Fig. 10). The decomposition rate of *p*-NP increases significantly as H_2O_2 dosage increases from 0.15 mM to 0.45 mM. More than 94.5% of *p*-NP disappears at 5 h when H_2O_2 concentrations are 0.45–0.75 mM. At 5 h, 65% and 35% *p*-NP were removed when the H_2O_2 dosage was 0.30 and 0.15 mM, respectively. Although the decomposition rate of *p*-NP increased with an increase of H_2O_2 dosage, no obviously changes were observed as H_2O_2 dosage was beyond 0.45 mM.

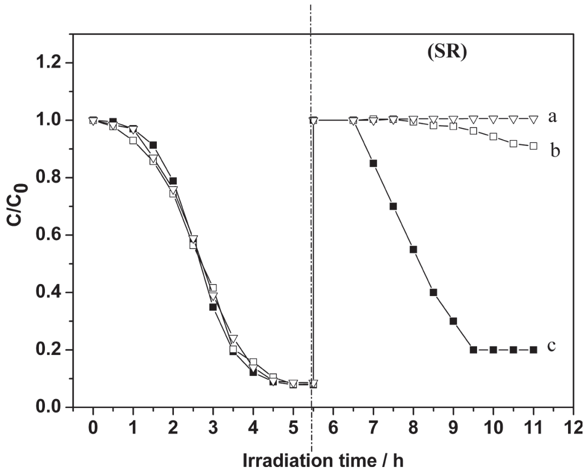

Figure 6. Changes of *p*-NP concentration versus reaction time. Without H_2O_2 under irradiation (a); with 0.45 mM H_2O_2 in the dark (b); with 0.45 mM H_2O_2 under irradiation (c) in the superadded reaction (SR) without extra addition of HQ.

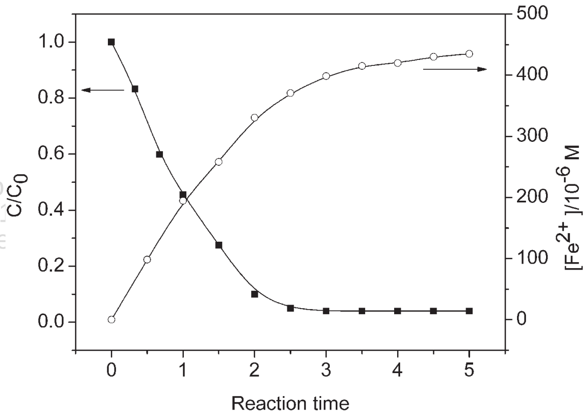

Figure 7. Changes of *p*-NP concentration (solid squares) and Fe(II) concentration (open circles) versus reaction time with the extra addition of HQ (0.03 mM).

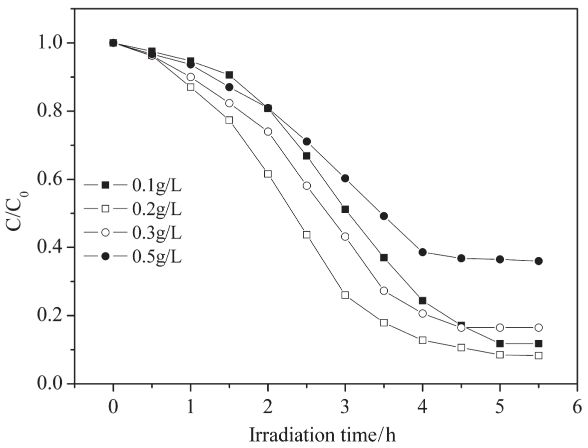

Figure 8. The effect of FH dosage on the decomposition rate of *p*-NP with 0.45 mM H_2O_2 under irradiation at pH 3.

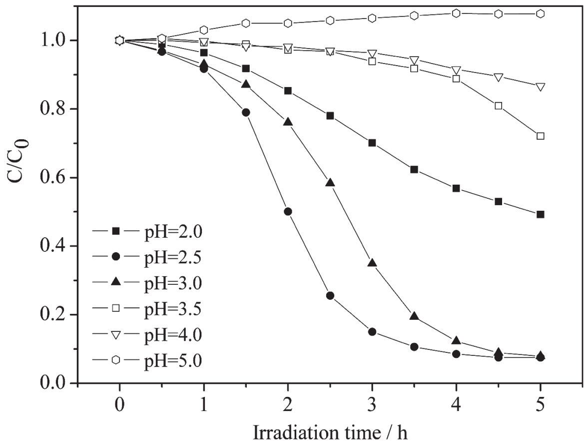

Figure 9. The removal of *p*-NP under different initial pH with 0.45 mM H_2O_2 and 0.2 $g \cdot L^{-1}$ FH under irradiation.

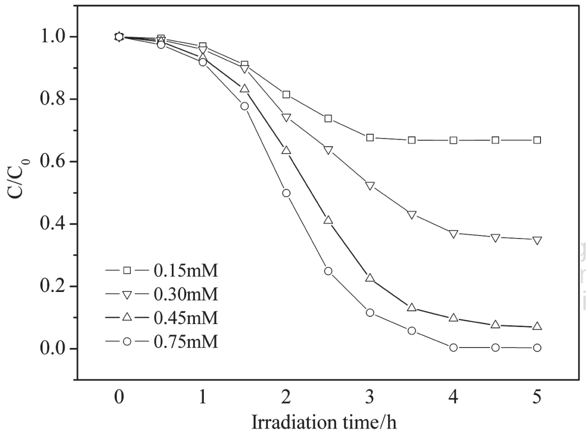

Figure 10. The decomposition rate of *p*-NP with different H_2O_2 dosage with 0.2 $g \cdot L^{-1}$ FH under irradiation at pH 3.

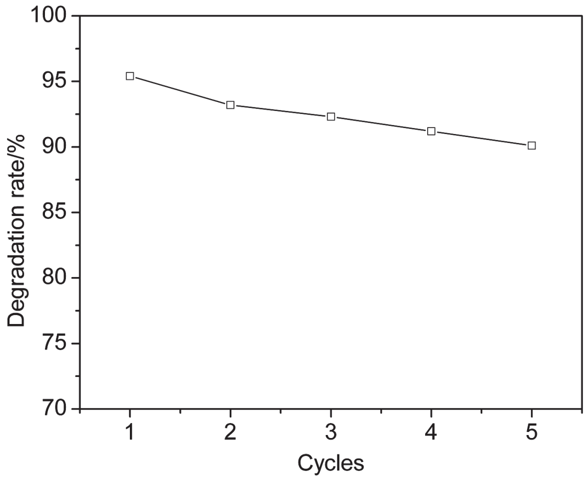

Figure 11. Degradation rate of *p*-NP in FH/H_2O_2 dispersions during the five cycles of photocatalytic oxidation.

Therefore, the optimum molar ratio of *p*-NP to H_2O_2 is 1:3.

3.2.5. *Reusability of FH*

In a wastewater treatment process, reusability of the catalyst is crucially important. To test the regeneration and reusability of FH, FH was used in five consecutive circles of photocalysis. As shown in Figure 11, the degradation rates of *p*-NP are 95.5%∼90% in the five consecutive cycles of photocatalytic oxidation, indicating that FH is of good reutilization.

4. CONCLUSIONS

This investigation illustrates the fact the combination of FH and trace H_2O_2 is effective for the degradation of *p*-NP under simulated sunlight irradiation. The combination of 0.2 $g \cdot L^{-1}$ FH, 0.45 mM of H_2O_2 is highly photoactive for the degradation of *p*-NP (0.15 mM) at pH 2.5–3.0. Hydroquinone, the initial intermediate of *p*-NP decomposition, autocatalyses the subsequent *p*-NP degradation due to its accelerating the photo-reductive dissolution of ferrihydrite. A ferrihydrite was reused several times, still keeping its original photocatalysis.

Acknowledgments: This work was supported by the National Natural Science Foundation of China (21077031).

References and Notes

1. M. H. Zhou and L. H. Lei, *Chemosphere* 63, 1032 **(2006)**.
2. L. L. Bo, X. Quan, and S. Chen, *Water Res.* 40, 3061 **(2006)**.
3. X. P. Zhu and J. R. Ni, *Electrochem. Commun.* 11, 274 **(2009)**.
4. Y. C Lin, C. F. Lin, and J. M. Chou, *J. Hazard. Mater.* 171, 452 **(2009)**.
5. K. P Wang, J. S. Guo, and M. Yang, *J. Hazard. Mater.* 162, 1243 **(2009)**.
6. J. P. Duguet and C. Anselme, *Ozone Sci. Tech.* 12, 281 **(1990)**.
7. H. Fenton, *Chem. Soc. Trans.* 65, 899 **(1894)**.
8. D. F Wang, Z. H. Wang, G. X. Ping, D. Chen, M. Q. Fan, L. Q. Bai, L. S. Qin, C. J. Lv, and K. Y. Shu, *Sci. Adv. Mater.* 5, 1642 **(2013)**.
9. J. Wang, F. Y. Qu, and X. Wu, *Sci. Adv. Mater.* 5, 1364 **(2013)**.
10. G. L.Huang, M. Jani, Y. L. Huang, and W. C. V. Yeh, *Sci. Adv. Mater.* 5, 1444 **(2013)**.
11. Q. Y. Li, L. L. Zong, Y. Y. Xing, X. D.Wang, L. G. Yu, and J. J. Yang, *Sci. Adv. Mater.* 5, 1316 **(2013)**.
12. R. K. Soni and M. P. Navas, *J. Nanoeng. Nanomanuf.* 3, 341 **(2013)**.
13. S. S. Arbuj, R. R. Hawaldar, U. P. Mulik, and D. P. Amalnerkar, *J. Nanoeng. Nanomanuf.* 3, 79 **(2013)**.
14. A. Goi and M. Trapido, *Chemosphere* 46, 913 **(2002)**.
15. Y. X. Du, M. H. Zhou, and L. C. Lei, *J. Hazard. Mater.* 136, 859 **(2006)**.
16. W. P. Kwan and B. M. Voelker, *Environ. Sci. Technol.* 36, 1467 **(2002)**.
17. W. P. Kwan and B. M. Voelker, *Environ. Sci. Technol.* 37, 1150 **(2003)**.
18. O. K. Borggaard, *J. Soil Sci.* 33, 443 **(1982)**.
19. D. R. Lovley, E. J. Phillips, and R. Potomac, *Appl. Environ. Microbiol.* 52, 751 **(1986)**.
20. R. M. Cornell and U. Schwertmann, 2nd edn., VCH, Weinheim, Germany **(2003)**, p. 106.
21. B. Dold, *Appl. Geochem.* 18, 1531 **(2003)**.

22. J. L. Jambor and J. E. Dutrizac, *Chem. Rev.* 98, 2549 (**1998**).
23. P. Wang and M. C. Lo, *Water Res.* 43, 3727 (**2009**).
24. D. Y. Tang, Z. Zheng, and K. Lin, *J. Hazard. Mater.* 143, 49 (**2007**).
25. Q. Yang, H. B. Xi, X. G. Wen, and Y. Qian, *Tech. Equip. Environ. Pollut. Control* 7, 50 (**2006**).
26. H. Bader, V. Sturzenegger, and J. Hoigne, *Water Res.* 22, 1109 (**1988**).
27. H. Fadrus, *J. Maly. Analyst* 100, 549 (**1975**).
28. V. A. Drits, B. A. Sakharov, and A. L. Salyn, *Clay Miner.* 28, 185 (**1993**).
29. S. J. Gregg and K. S. W. Sing, Adsorption, Surface Area and Porosity, Seconded, Academic Press, London (**1995**), p. 200.
30. C. Sangwichien, G. L. Aranovich, and M. D. Donohue, *Colloids Surf. A*: *Physicochem. Eng. Aspects* 206, 313 (**2002**).
31. Y. Wang, Y. C. Zhao, and Y. Ma, *J. Mol. Catal. A*: *Chem.* 325, 79 (**2010**).
32. J. C. Barreiro, M. D. Capelatoa, and L. N. Martin, *Water. Res.* 41, 55 (**2007**).
33. Y. Li, H. Fang, S. Liang, and Z. Wang, *Chin. J. Anal. Chem.* 36, 95 (**2008**).
34. S. F. Zhao, H. J. Ma, and M. Wang, *J. Hazard. Mater.* 180, 86 (**2010**).
35. C. P. Huang, C. P. Chen, and Y. F. Huang, *J. Mole. Cata. A Chem.* 304, 121 (**2009**).
36. T. D. Waite and F. M. Morel, *Environ. Sci. Technol.* 18, 860 (**1984**).
37. C. Siffert and B. Sulzberger, *Langmuir* 7, 1627 (**1991**).
38. M. T. Goncalves and O. Campos, *Chemosphere* 39, 781 (**1999**).
39. M. E. Taha, M. R. Yasser, and H. M. Zeinhom, *J. Hazard. Mater.* 174, 352 (**2010**).
40. K. Kuma, S. Nakabayashi, and K. P. Matsunaga, *Water Res.* 29, 1559 (**1995**).
41. B. M. Voelker, F. M. Morel, and B. Sulzberger, *Environ. Sci. Technol.* 31, 1004 (**1997**).
42. K. M. Cunningham, M. C. Goldberg, and E. R. Weiner, *Environ. Sci. Technol.* 22, 1090 (**1988**).

Received: 3 November 2012. Accepted: 4 March 2013.